


# Study on Temperature and Water Turbulence Impact on Saline Water-Based Wireless Optical Communication

Shofuro Afifah <sup>1</sup>, Amirullah Wijayanto <sup>1</sup>, Ya-Ling Liu <sup>1</sup>, Shien-Kuei Liaw <sup>1,2,\*</sup>, Pei-Jun Lee <sup>2</sup>, Chien-Hung Yeh <sup>3</sup>  and Ochi Hiroshi <sup>4</sup>

<sup>1</sup> Graduate Institute of Electro-Optical Engineering, National Taiwan University of Science and Technology, Taipei 10607, Taiwan

<sup>2</sup> Department of Electronics and Computer Engineering, National Taiwan University of Science and Technology, Taipei 10607, Taiwan

<sup>3</sup> Department of Photonics, Feng Chia University, Taichung 40724, Taiwan

<sup>4</sup> Department of Computer Science and Network, Kyushu Institute of Technology, Fukuoka 804-0015, Japan

\* Correspondence: skliaw@mail.ntust.edu.tw

**Abstract:** Underwater wireless optical communication (UWOC) is a promising solution for Gb/s rate and long-distance underwater communication. However, random changes in the local temperature and salinity of seawater have caused different refractive indices of ocean water. This study investigated the UWOC system in different saline water while simultaneously changing the temperature and water flow. A maximum bit error rate (BER) of  $4.851 \times 10^{-6}$  was measured at  $-7.41$  dBm in 3 m of 45.56 g/L saline water. By changing the temperature to 30 °C, the bit error rate (BER) value reached  $5.12 \times 10^{-6}$  in the saline water. On the other hand, water flow was generated in various types of water salinity to compare simultaneous environmental effects in the UWOC system. In 45.56 g/L of saline water with water flow, the UWOC system was still capable of reaching a BER value of  $4 \times 10^{-4}$ .

**Keywords:** underwater wireless optical communication; BER; saline water; environmental factors



**Citation:** Afifah, S.; Wijayanto, A.; Liu, Y.-L.; Liaw, S.-K.; Lee, P.-J.; Yeh, C.-H.; Hiroshi, O. Study on Temperature and Water Turbulence Impact on Saline Water-Based Wireless Optical Communication. *Photonics* **2023**, *10*, 383. <https://doi.org/10.3390/photonics10040383>

Received: 16 January 2023

Revised: 25 March 2023

Accepted: 28 March 2023

Published: 30 March 2023



**Copyright:** © 2023 by the authors. Licensee MDPI, Basel, Switzerland. This article is an open access article distributed under the terms and conditions of the Creative Commons Attribution (CC BY) license (<https://creativecommons.org/licenses/by/4.0/>).

## 1. Introduction

Long-distance and high data transmission in wireless optical communication has been an exciting topic that has been developed by many researchers in recent years. Optical wireless communication (OWC) transmits information or data received by the detector through a free-space medium. So far, in our lab, the data transmission medium for the OWC system has already been measured in the air [1], water [2], and hybrid mode [3]. Many researchers have investigated OWC in an underwater medium. Light wavelengths and radio frequency [4,5] are usually used to transmit data in underwater communication.

Underwater wireless optical communication (UWOC) plays a vital role in ocean communication, military, education, and many fields that connect several parts of the world. UWOC can obtain high data rate transmission [6–8], low optical power consumption [9], and secure information [10]. It refers to a wireless data transmission that uses the light wavelength as the optical link in the medium underwater. Due to its high bandwidth and immunity to electromagnetic interference, visible light communication (VLC) is the preferred communication technology. Recently, researchers have conducted a study in UWOC using a high-speed communication bandwidth over a wide range of distances. Most experiments were conducted in clear or tap water; however, only a few measurements were conducted in the research on seawater salinity. In seawater, environmental changes such as the temperature [11], water flow [12], and salinity of water [13] cause attenuation in the UWOC. Random changes in the local temperature and salinity of seawater cause unexpected fluctuations in the refractive index of ocean water [14]. This study investigated UWOC performance in different water salinity. As we know, when water has more particles

dissolved, the salinity is higher, and the water becomes turbid. In our experiment, we measured the water with different types of salinity to compare the impact on the UWOC system. Chao Li et al. proposed a high-sensitive long-reach UWOC system with an Mbps-scale data rate across a 10 m underwater channel. Their experiment investigated different water types, and the maximum distance that the 2 Mbps signal could be extended up to was 100 m in the first type ( $c = 0.056 \text{ m}^{-1}$ ) of seawater [15]. Tian et al. proposed a blue gallium nitride (GaN) micro-light-emitting-diode (micro-LED)-based UWOC system at a distance of 2.3 m with a maximum data rate of 790 Mbps. They found that as sea salt, Maalox, and chlorophyll increased, it affected the light attenuation mechanism [16]. Therefore, we measured the UWOC system in various types of salinity by using 155 Mbps, 622 Mbps, and 1.25 Gbps to compare the environmental impact at a 3 m distance.

In our previous work [2], tap water was used to measure the impact of temperature and turbulence (water flow) issues; we did not study temperature issues on seawater or the various types of salinity experiments. This paper further discusses the impact of saline water on the UWOC system with two simultaneous and changing environmental factors such as temperature (or water flow) and various types of saline water. Furthermore, the transmission channel in saline water could degrade the light beam's power more than in tap water, which could impact the data transmission's quality.

## 2. Experimental Scheme

Underwater wireless optical communication consists of the transmitter, channel path, and receiver side. The proposed scheme is shown in Figure 1 below:

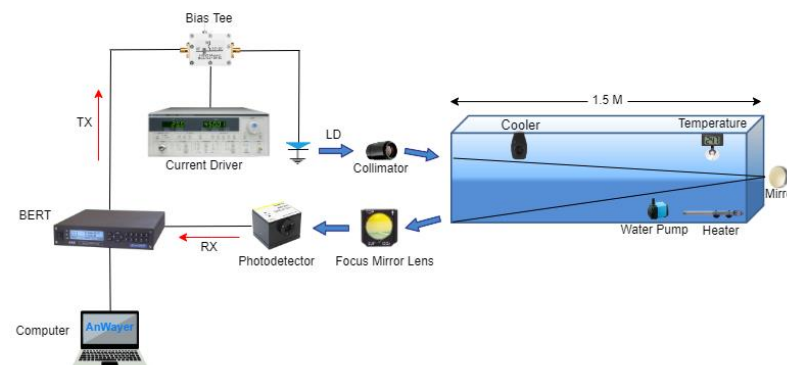


**Figure 1.** UWOC experimental scheme for environmental measurement.

The experiment scheme consists of the transmitter, medium, and receiver. At the transmitter side, a current driver (ILX Lightwave LDC3722, ILX Lightwave Corporation, Bozeman, US) drove the current to the blue laser diode (OSRAM PL450 TO-38, OSRAM Licht AG, Munich, Germany). The laser diode (LD) used collimation to focus the light and a cooler to control the laser temperature. The light was transmitted through a  $1.5 \text{ m} \times 0.3 \text{ m} \times 0.3 \text{ m}$  size water tank. Secondly, the medium was seawater with different types of salinity. The heater, fan, and water pump were placed inside the tank to vary the temperature and water condition. A digital thermometer showed the temperature measurement inside the water tank. Then, an optical mirror reflected the laser beam and expanded the transmission distance to 3 m. In the receiver part, the focus mirror lens and avalanche photodiode (APD 210, Menlo System GmbH, Martinsried, Germany) were used to receive the laser beam. Then, the information signal was evaluated using a bit error rate test (BERT). The modulation in this experiment used NRZ-OOK. This experiment used a pseudorandom binary sequence 7 with a repetition period of 127 values. The equation can be found in  $N = 2^k - 1$ , where 'k' indicates the size of random data for each sequence. For a maximum length sequence, where  $N = 2^k - 1$ , the duty cycle is  $\frac{1}{2}$ . A bias tee was used to superimpose a modulation current onto the laser diode DC-supply current, thereby modulating the output power of the laser. The modulation speed was 1.25 Gbps, and the signal generator could modulate up to 2.5 Gbps. Due to limitations in our laboratory, the APD frequency could only receive

modulations up to 1.25 Gbps. In the demodulation part, we used a Photodetector (Menlo System GmbH, Martinsried, Germany) APD 210 to change the optical signal to an electrical signal. The BERT measurement was used to compare the modulated signal transmitted and the demodulated signal received by the photodetector. The relationship between salinity, mass, and volume is shown in the equation below:

$$\text{Salinity} = \frac{\text{Mass}}{\text{Volume}}, \quad (1)$$

As shown in Equation (1), the salinity value is mass (g) divided by volume (L). When the salt was dissolved in the tap water, salinity increased. Therefore, the amount of mass added to a particular volume of water increases the salinity of the water. The authors did measure using a hydrometer first to see the density in the hydrometer scale. Since there may have been undissolved salt inside the water tank, the extra salt could have drowned in the bottom of the water tank. The hydrometer scale of seawater was around 1.025 at 25 °C and 37 salinity in parts per 1000 [17]. The volume was obtained by multiplying the width 0.3 m × length 1.5 m × height 0.12 m; the result was 54 L.

Based on Table 1, sea salt was added to vary the environment of the water in this experiment. In our experiment, the salinity of water, based on the hydrometer scale, was 1.03 by adding 45.56 g/L sea salt into the tap water. The water tank was filled with salt water, and a hydrometer was used to measure water salinity, as shown in Figure 2. Typically, the salinity increases from the ocean’s surface to deep water; thus, the saltwater density increases as seawater depth increases at a constant temperature (R1Q3). Based on the halocline or a vertical salinity gradient, low-salinity water floats on top of high-salinity water. When the density increases, the amount of salt in the water, or salinity, also increases. Many factors may change the seawater density. Whether the polar ice is melting or frozen can affect salinity. The sea salt was evenly distributed. A salinity of 22.78 g/L or density of 1.01 was in the surface or mixed layer; a salinity of 37.96 g/L or density of 1.02 was in the depth of 0–500 m; the salinity of 45.56 g/L or density of 1.03 was in the depth of 500–2500 m. The depth of the ocean can be identified by salinity and temperature. For example, near the surface, the salinity is low, and the temperature is high. This is influenced by sunshine and the greenhouse effect.

**Table 1.** Water salinity measurements at various hydrometer scales.

Hydrometer Scale	Salinity (g/L)	Salt Added (g)	Volume (L)
1.01	22.78	1230	54
1.02	37.96	2050	54
1.03	45.56	2460	54

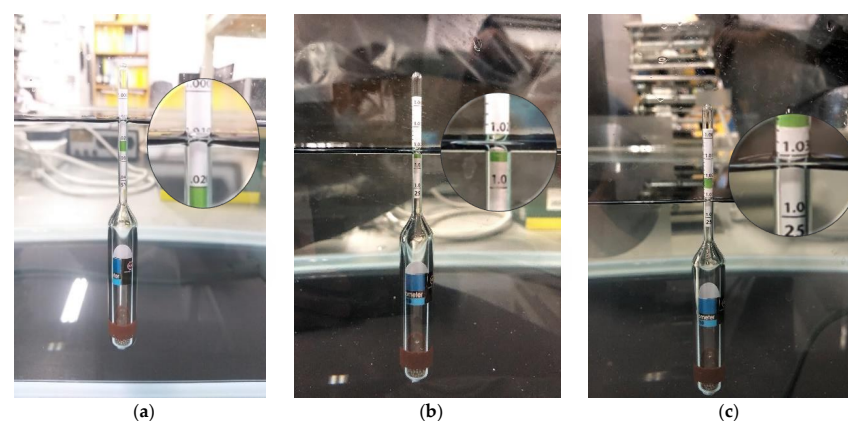


**Figure 2.** The hydrometer measurement of different types of water salinity: (a) 1.01; (b) 1.02; and (c) 1.03 hydrometer scale.

### 3. Measurement Results

#### 3.1. The UWOC System in Different Water Conditions

In this experiment, a 450 nm blue-light laser beam was transmitted in different mediums, such as free space, tap water, and seawater. The different refractive indexes caused the scintillation of the focused laser beam, which caused signal fading and beam wandering in the transmission channel. This experiment was measured at a 1.5 m distance. The distance measurement of 1.5 m was used to compare measurements of the UWOC system in tap water, seawater, and free space with no additional loss from the mirror. The threshold current was around 15 mA using OSRAM PL-450B. As shown in Figure 3, when the blue LD had a typical drive current of 100 mA, the optical power of tap water decreased by about 21.6% compared to the free space medium. In 45.56 g/L of saline water, the laser optical power was reduced by approximately 58.62% compared to the tap water. The optical power decreased by about 80.22% in total because of the different mediums of seawater. Some of the factors involved in attenuating laser optical power were the transmission distance, the wavelength used in the UWOC system, and the different refractive indexes in the air and water.

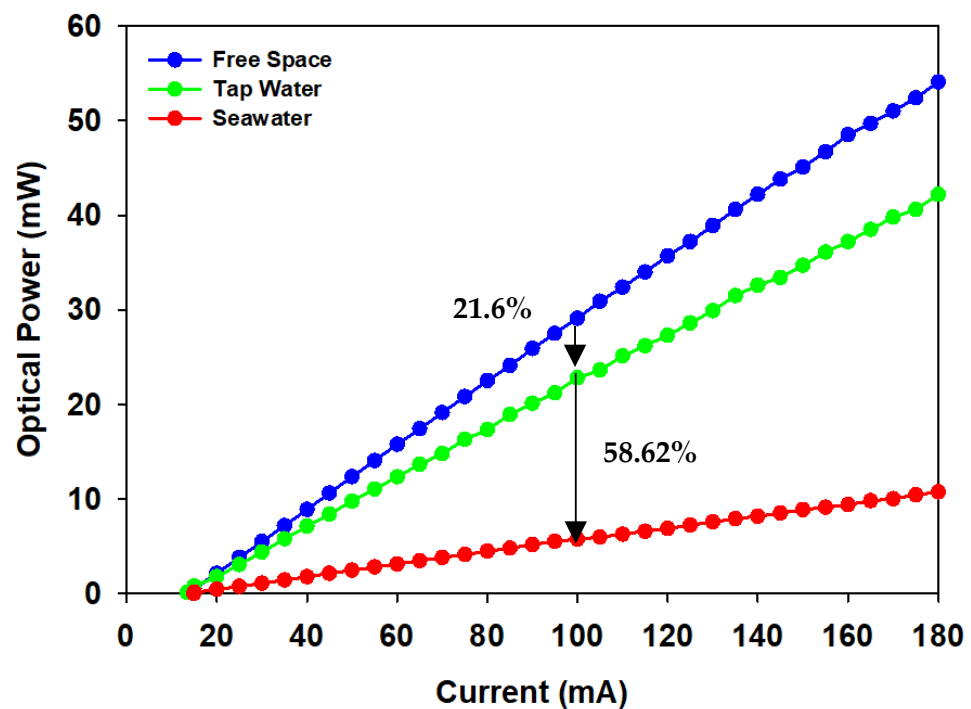
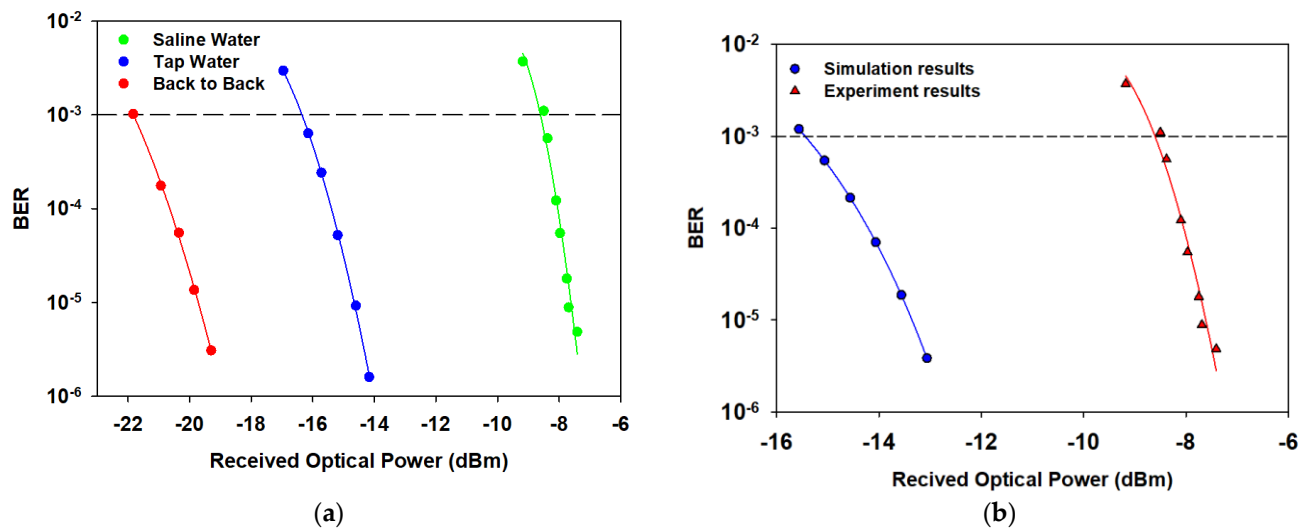


Figure 3. Laser attenuation in a different medium of transmission.

In Figure 4a, we measured the bit error rate (BER) curve of the tap water and seawater at a distance of 1.5 m. Know that, the value of hyphen (-) in the x axis defined as a minus sign from the Sigmaplot software. The explanation is the same for some of the following figures. The back-to-back measurement was measured directly from the LD into the APD without the medium of water. This experiment aimed to find the optical power difference between the tap and seawater to reach the maximum BER. Scattering and absorption in the seawater were significant reasons for the signal attenuation. The forward error correction (FEC) value for underwater communication was around  $10^{-3}$ . In the FEC limit line, the BER value recorded for the back-to-back system was  $1.022 \times 10^{-3}$  at 21.83 dBm (R1Q4). The BER value of tap water at a  $-16.96$  dBm receiving power was  $2.97 \times 10^{-3}$ . The BER value of saline water was  $3.72 \times 10^{-3}$  at a  $-9.18$  dBm receiving power. The difference in the receiving power between tap water and sea water at  $10^{-3}$  was 7.78 dB (R1Q1). The BER measurement of the UWOC system in the seawater needed more optical power than in tap water. However, the BER curve in seawater had a nearly vertical graph, indicating

that BER could drift to the worst by only minor changes in optical power. Figure 4b shows the BER comparison between the Optisystem 13 simulation and experimental saline water-based UWOC system measurement. The difference in the receiving power between the experimental and simulation study was 5.65 dB at BER of  $3 \times 10^{-6}$  (R1Q1).



**Figure 4.** (a) BER measurements in different types of water with 1.25 Gbps modulation speed; and (b) the BER comparison of UWOC system in the simulation and experiment.

### 3.2. Seawater Salinity and Temperature Combination

In seawater, different areas have different temperatures. Seawater temperature is affected by factors such as sunlight, atmospheric heat transfer, turbidity, and water depth. It also changes from place to place and from one season to another [18]. The temperature effect makes it possible for researchers to simulate the temperature of the actual ocean inside a laboratory. Ocean water with a median salinity of 35 psu freezes at  $-1.94$  degrees Celsius (28.5 degrees Fahrenheit). Therefore, it follows that sea ice can form at high latitudes. The average temperature of water at the ocean's surface is about 17 degrees Celsius (62.6 degrees Fahrenheit) [19]. As the temperature increases, the salinity of water decreases. Therefore, we measured the impact of temperature changes on seawater density.

A heater was turned on to reach a specific temperature, as shown in the digital thermometer, for higher temperature measurements. The lower temperature measurement used a cooler fan to generate a wind breeze and an ice pack inside the water. The temperature within the water tank changed automatically based on the temperature measurement tool. We conducted the experiment while the temperature automatically increased to the desired level. The heater and cooler fan made the temperature stable; however, the water temperature was non-uniform. The non-uniform water temperature caused the water to move in a turbulent manner, which was similar to realistic conditions in the ocean. The water tank could have had a temperature variation up to  $\pm 2$  °C; therefore, the optical attenuation in the water was increased due to non-uniform water refractive indices and non-uniform water temperatures. Each measurement was taken under the same environmental factors, and different data rates resulted in different BERs. Therefore, the data rate caused signal distortion as higher speeds led to faster modulation. In this experiment, we used data rates of 155 Mbps, 622 Mbps, and 1.25 Gbps.

The graphs in Figure 5, for 155 Mbps and 622 Mbps, were nearly identical. The 1.25 Gbps drifted to a higher and worse BER even though it was still receiving higher optical power. In Figure 5, the 1.25 Gbps BER floor slightly changed as the temperature increased. The modulation speed of 155 Mbps and 622 Mbps was slightly different since the range was still in the ~Mbps. In the ~Gbps order of modulation speed, the noise of the information signal increased, which could have impacted the attenuation in the UWOC system. When



the modulation speed increased, the optical power also needed to be higher. The BER floor at a lower temperature of 15 °C was  $1.07 \times 10^{-5}$ , while at a higher temperature of 30 °C, the BER floor reached up to  $5.12 \times 10^{-6}$ . As we know, ocean temperature changes and is non-uniform, along with the depth of the ocean. Temperature decreases while depth increases. Based on the Thermocline (a layer within a body of water or air where the temperature changes rapidly along with depth), a temperature of 15 °C is around 600 m in depth, 26 °C is around 20–80 m depth in the summertime, and the highest ocean temperature is 30 °C on the surface. A higher temperature affects a lower salinity which can lower the density of seawater. In this measurement, the optical power slightly differed in various temperatures. Therefore, the UWOC system could still reach the information in seawater salinity with different temperatures. The main cause of optical signal fading in a typical UWOC channel is temperature or salinity-induced turbulence [20]. Therefore, we provide the statistical distribution of received optical power due to temperature changes in Figure 6. The received optical signal faded as the temperature increased. Figure 7 shows the time in the bit period against the received amplitude in various temperatures. Considering the high data rate of 1.25 Gbps used in this paper, the channel coherence time of the signal amplitude was relatively slow, fading in the 0.2 to 1-bit period as the temperature increased.

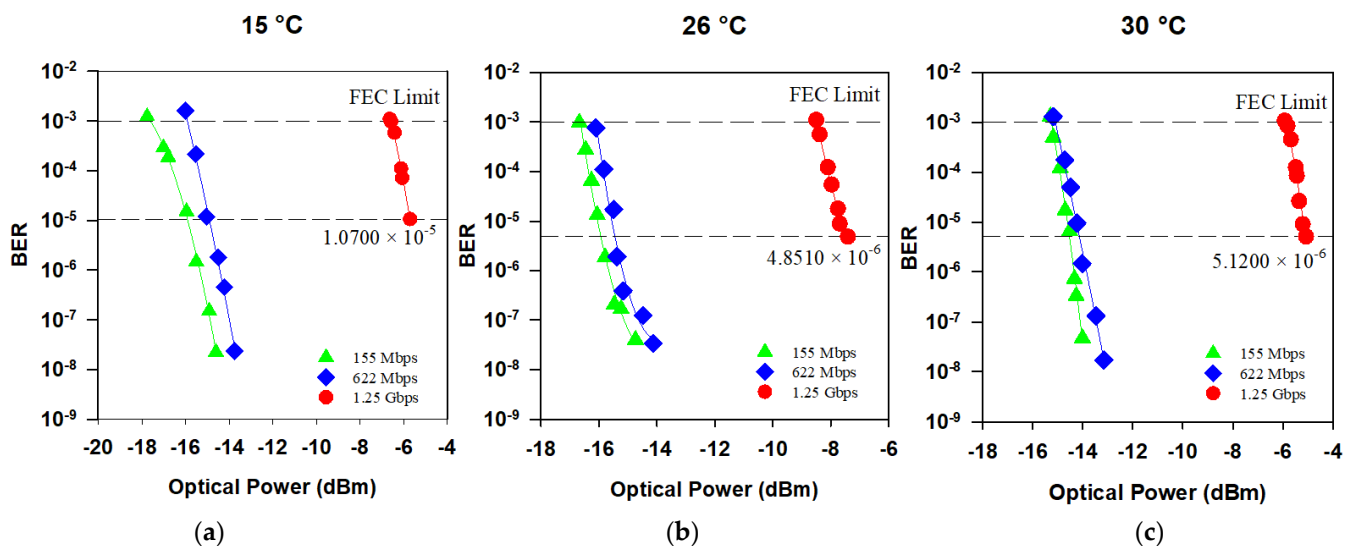


Figure 5. The BER comparison in different temperatures: (a) 15 °C; (b) 26 °C; and (c) 30 °C.

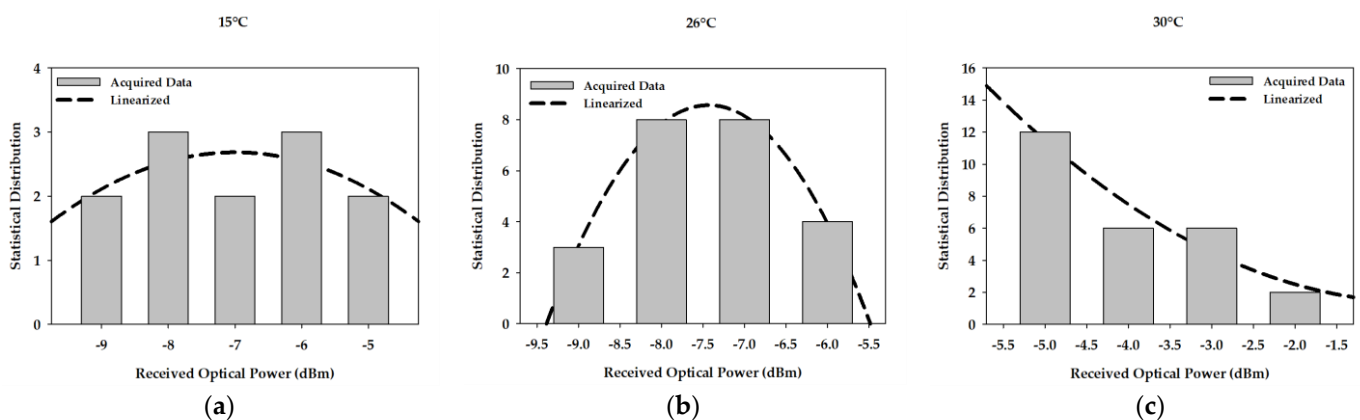
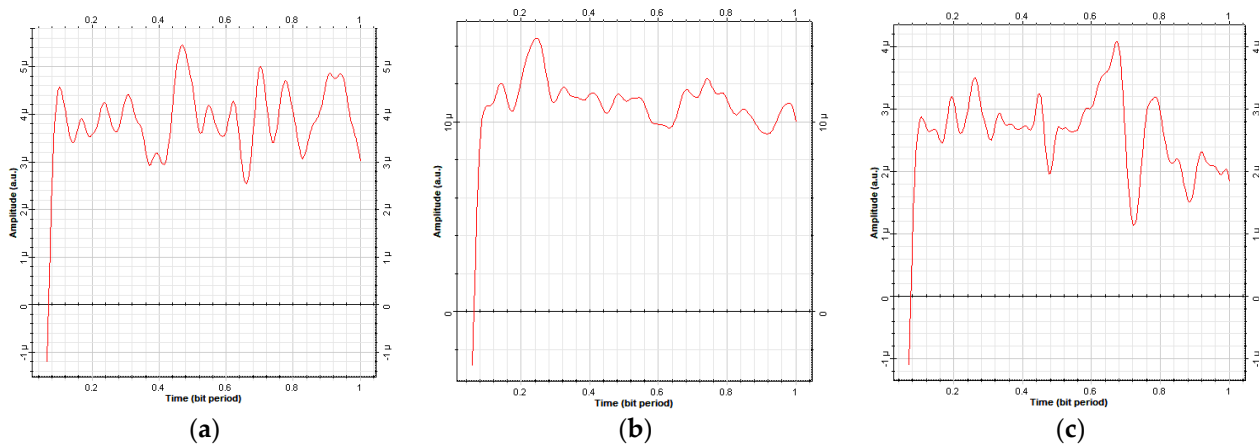


Figure 6. Statistical distribution of received optical power due to temperature changes: (a) 15 °C, (b) 26 °C, and (c) 30 °C (R4Q2).



**Figure 7.** Time (bit period) against received power amplitude in various temperatures: (a) 15 °C, (b) 26 °C, and (c) 30 °C.

### 3.3. Seawater Salinity and Water Turbulence Combination

A motor pump with 1200 L/h speed was placed inside the water tank to simulate water flow in the water tank. The water turbulence (flow) caused small particles to float around the entire water tank. In oceanic water flow, temperature and salinity fluctuations are the main factors influencing a laser beam's propagating properties [21,22]. Underwater water flow can be defined as random refractive index variations that affect the beam propagation through the transmission path. Based on [23], when the water pump is turned on, the bubble breaking increases due to high flow rates. The quicker the water flow is moving, the more particles are visible in the signal light path, and these impurities soon float throughout the entire water tank. The difference in the −9 dBm transmitter power was needed to gain the same received power when the pump was turned off. The UWOC system design could be significantly changed depending on the salinity and size of air bubbles in the optical link. The water flow was measured in different hydrometer scales of 1.01, 1.02, and 1.03 to compare with the UWOC system performance. Some undissolved sea salt and dust made the UWOC system worse. The laser beam became unclear as the tiny particles floated around the water. This phenomenon caused attenuation in the UWOC transmission system. The data rate was generated using NRZ OOK modulation. This measurement aimed to compare the difference between data rates in general.

As shown in Figure 8, in 22.78 g/L saline water, the best BER of  $8 \times 10^{-6}$  was obtained when the motor pump was turned on, and the best BER of  $3 \times 10^{-6}$  was obtained when turning off the motor pump. In 37.96 g/L saline water, the BER reached  $3 \times 10^{-5}$  and  $4 \times 10^{-6}$ , respectively, when turning the motor pump on and off. Moreover, as the hydrometer scale increased to 1.03, or in the 45.56 g/L saline water, smaller floating particles caused different refractive indexes. When turning it on and off, the motor pump drifted into  $4 \times 10^{-4}$  and  $5 \times 10^{-6}$ , respectively. The seawater salinity contributed to the UWOC system attenuation and degraded the signal. Figure 9 shows the statistical distribution of the received optical power due to the water flow changes in various water densities. Figure 10 shows the time (bit period) against the received power amplitude due to water flow changes in various water densities of 1.01, 1.02, and 1.03. As water salinity increased simultaneously with the water flow, the channel coherence time of the amplitude signal had more fluctuations in the 0.2 to 1-bit period. As the salinity increased, the signal distribution became large, indicating the signal fading condition. Figure 11 shows the channel estimation for each water flow measurement.

$$P_{rx} = P_{tx} \times H, \quad (2)$$

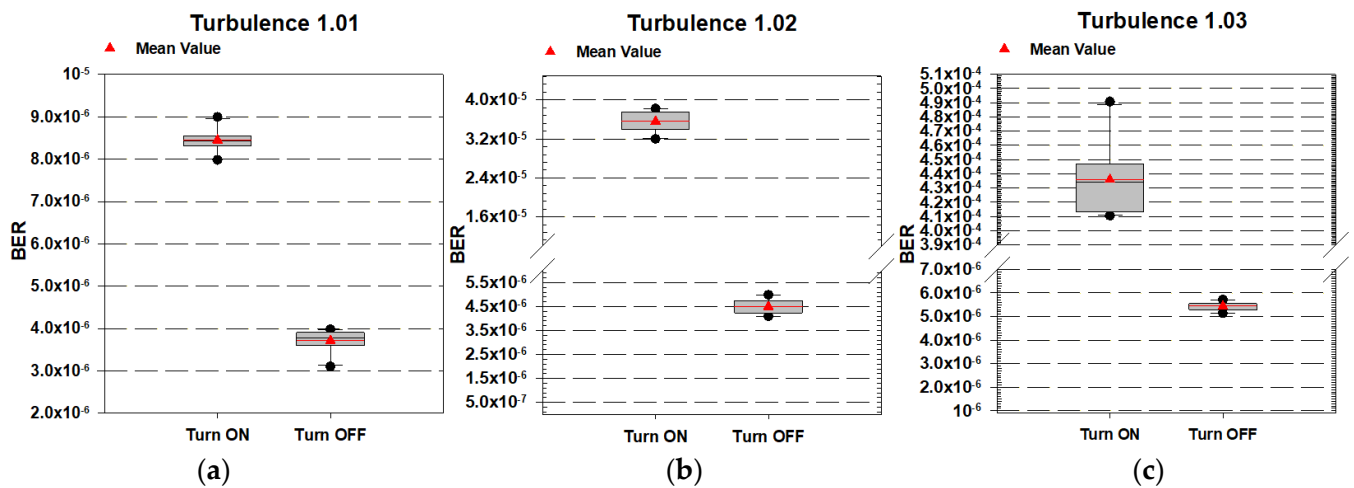


**Figure 8.** The water flow measurements for different types of water: (a) 22.78 g/L; (b) 37.96 g/L; and (c) 45.56 g/L.

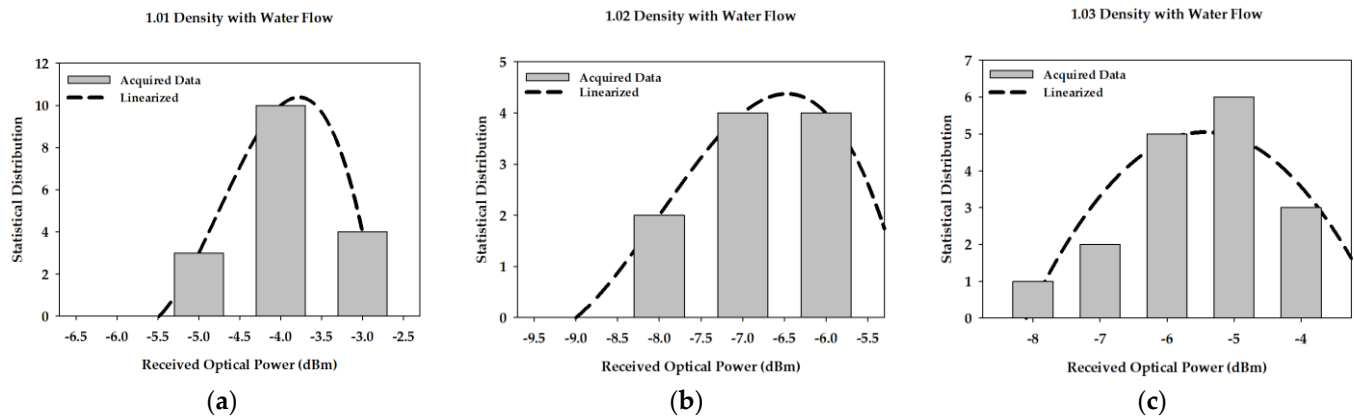


**Figure 9.** Statistical distribution of received signal amplitude due to water flow changes in various water densities: (a) 1.01 density, (b) 1.02 density, and (c) 1.03 density (R4Q2).

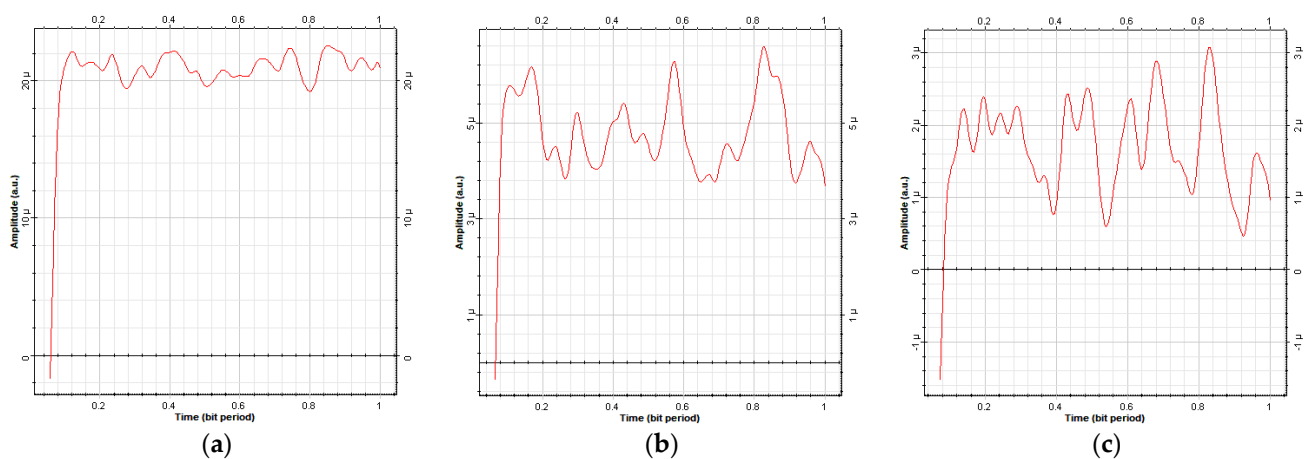


**Figure 10.** Time (bit period) against received power amplitude due to water flow changes in various water densities: (a) 1.01 density, (b) 1.02 density, and (c) 1.03 density.



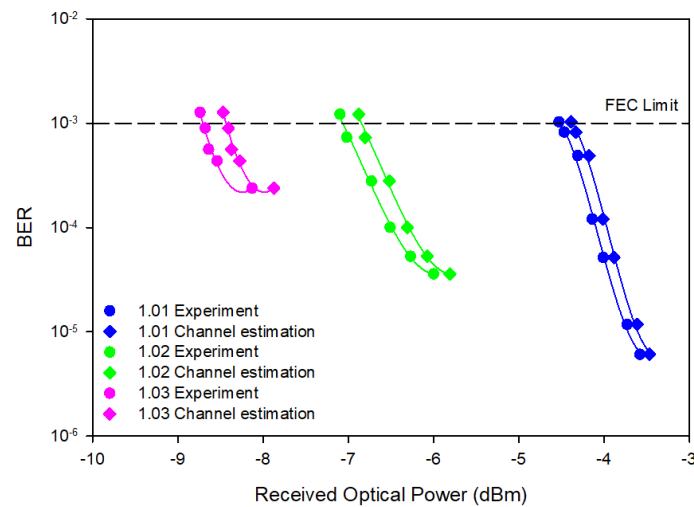


**Figure 11.** Channel estimation for each water flow measurement.

The channel estimation was obtained by Equation (2), where  $P_{rx}$  is the received power,  $P_{tx}$  is the transmitted power, and  $H$  is the number of the channel.

#### 4. Conclusions

This paper measured and evaluated the UWOC system in different types of seawater salinity alongside simultaneous environmental factors, such as turbulence and water flow, using a 450 nm blue-light LD. The saline water was measured at 22.78 g/L, 37.96 g/L, and 45.56 g/L by adding sea salt into the water tank. The 45.56 g/L saline water could reach a maximum bit error rate (BER) of  $4.851 \times 10^{-6}$  at  $-7.41$  dBm at a 3 m distance. In 45.56 g/L saline water, the optical power decreased by about 80.22% more than in tap water. The UWOC system was also evaluated in various water temperatures ranging from  $15$  °C to room temperature (Typ.  $26$  °C) until  $30$  °C. As the temperature increased to  $30$  °C, the BER degraded to  $5.12 \times 10^{-6}$ . The water temperature was non-uniform, causing a different refractive index and higher attenuation. Water flow was generated in the various types of water salinity to compare simultaneous environmental effects in the UWOC system. In the 45.56 g/L saline water with water flow, the UWOC system was still capable of reaching a BER of  $4 \times 10^{-4}$ . The seawater salinity contributed to the UWOC system's attenuation and degraded the signal. The differences between the simulation and experiment for UWOC were compared in this study, in conjunction with the results comparing salinity in seawater with various densities.

**Author Contributions:** Methodology, S.A. and S.-K.L.; validation, P.-J.L. and C.-H.Y.; experiment, S.A., A.W., and Y.-L.L.; data curation, A.W.; writing—original draft preparation, S.A. and Y.-L.L.; writing—review and editing, S.-K.L. and O.H. All authors have read and agreed to the published version of the manuscript.

**Funding:** The work is supported by the National Science and Technology Council, Taiwan, under Grant NSTC 110-2224-E-011-004, NSTC 110-2221-E-011-109, and NSTC 111-2224-E-006-008. This work is also supported by the joint project under Grant Kyutech-NTUST-111-05.

**Institutional Review Board Statement:** Not applicable.

**Informed Consent Statement:** Not applicable.

**Data Availability Statement:** Not applicable.

**Acknowledgments:** The authors would like to thank Jane Liao, T.Y. Lin, Brian Pamukti, Lina Marlina, and M. Fajar Faliasthiunus P. for their kind help and support.

**Conflicts of Interest:** The authors declare no conflict of interest.

## References

1. Hsu, H.; Lu, W.C.; Minh, H.L.; Ghassemlooy, Z.; Yu, Y.L.; Liaw, S.K.  $2 \times 80$  Gbit/s DWDM bidirectional wavelength reuse optical wireless transmission. *IEEE Photon. J.* **2013**, *5*, 7901708.
2. Li, D.C.; Chen, C.C.; Liaw, S.K.; Afifah, S.; Sung, J.Y.; Yeh, C.H. Performance evaluation of underwater wireless optical communication system by varying the environmental parameters. *Photonics* **2021**, *8*, 74. [\[CrossRef\]](#)
3. Yu, Y.L.; Liaw, S.K.; Chou, H.H.; Hoa, L.M.; Ghassemlooy, Z. A hybrid optical fiber and FSO system for bidirectional communications used in bridges. *IEEE Photon. J.* **2015**, *7*, 6. [\[CrossRef\]](#)
4. Lv, Z.; He, G.; Yang, H.; Chen, R.; Li, Y.; Zhang, W.; Qiu, C.; Liu, Z. The Investigation of Underwater Wireless Optical Communication Links Using the Total Reflection at the Air-Water Interface in the Presence of Waves. *Photonics* **2022**, *9*, 525. [\[CrossRef\]](#)
5. Rycroft, S.; Shaw, A.; Fergus, P.; Kot, P.; Hashim, K.; Moody, A.; Conway, L. A first implementation of underwater communications in raw water using the 433 MHz frequency combined with a bowtie antenna. *Sensors* **2019**, *19*, 1813. [\[CrossRef\]](#)
6. Sait, M.; Trichili, A.; Alkhazragi, O.; Alshaibaini, S.; Ng, T.K.; Alouini, M.S.; Ooi, B.S. Dual-wavelength luminescent fibers receiver for wide field-of-view, Gb/s underwater optical wireless communication. *Opt. Express* **2021**, *29*, 38014–38026. [\[CrossRef\]](#)
7. Huang, Y.F.; Tsai, C.T.; Chi, Y.C.; Huang, D.W.; Lin, G.R. Filtered Multicarrier OFDM Encoding on Blue Laser Diode for 14.8-Gbps Seawater Transmission. *J. Light. Technol.* **2018**, *36*, 1739–1745. [\[CrossRef\]](#)
8. Wei, D.; Qi, C.; Huang, C.; Chen, J.; Song, A.; Song, G.; Pan, M. Riding stress wave: Underwater communications through pipeline networks. *IEEE J. Ocean. Eng.* **2021**, *46*, 1450–1462. [\[CrossRef\]](#)
9. Liu, X.; Yi, S.; Zhou, X.; Fang, Z.; Qiu, Z.-J.; Hu, L.; Cong, C.; Zheng, L.; Liu, R.; Tian, P. 34.5 m underwater optical wireless communication with 2.7 Gbps data rate based on a green laser diode with NRZ-OOK modulation. *Opt. Express* **2017**, *25*, 27937–27947. [\[CrossRef\]](#)
10. Tang, X.; Chen, Z.; Zhao, Z.; Kumar, R.; Dong, Y. Experimental study on underwater continuous-variable quantum key distribution with discrete modulation. *Opt. Express* **2022**, *30*, 32428–32437. [\[CrossRef\]](#)
11. Oubei, H.-M.; Zedini, E.; ElAfandy, R.-T.; Kammoun, A.; Abdallah, M.; Ng, T.-K.; Hamdi, M.; Alouini, M.-S.; Ooi, B.S. Simple statistical channel model for weak temperature-induced turbulence in underwater wireless optical communication systems. *Opt. Lett.* **2017**, *42*, 2455–2458. [\[CrossRef\]](#) [\[PubMed\]](#)
12. Yang, H.; Yan, Q.; Wang, P.; Hu, L.; Zhang, Y. Bit-error rate and average capacity of an absorbent and turbulent underwater wireless communication link with perfect Laguerre-Gauss beam. *Opt. Express* **2022**, *30*, 9053–9064. [\[CrossRef\]](#) [\[PubMed\]](#)
13. Ata, Y.; Yao, J.; Korotkova, O. BER variation of an optical wireless communication system in underwater turbulent medium with any temperature and salinity concentration. *Opt. Commun.* **2021**, *485*, 126751. [\[CrossRef\]](#)
14. Ji, X.; Yin, H.; Jing, L.; Liang, Y.; Wang, J. Modeling and performance analysis of oblique underwater optical communication links considering turbulence effects based on seawater depth layering. *Opt. Express* **2022**, *30*, 18874–18888. [\[CrossRef\]](#)
15. Li, C.; Liu, Z.; Chen, D.; Deng, X.; Yan, F.; Li, S.; Hu, Z. Experimental demonstration of high-sensitivity underwater optical wireless communication based on photocounting receiver. *Photonics* **2021**, *8*, 467. [\[CrossRef\]](#)
16. Tian, P.; Chen, H.; Wang, P.; Liu, X.; Chen, X.; Zhou, G.; Zhang, S.; Lu, J.; Qiu, P.; Qian, Z.; et al. Absorption and scattering effects of Maalox, chlorophyll, and sea salt on a micro-LED-based underwater wireless optical communication. *Chin. Opt. Lett.* **2019**, *17*, 100010. [\[CrossRef\]](#)
17. Service, J.H. *Measurement of Salinity of Seawater*; United States Government Printing Office: Washington, DC, USA, 1928.
18. El Banna, A.; Wu, K.; El Halawany, B.M. Opportunistic cooperative transmission for underwater communication based on the water's key physical variables. *IEEE Sens. J.* **2020**, *20*, 2792–2802. [\[CrossRef\]](#)
19. Windows to the Universe. *Temperature of Ocean Water*; National Earth Science Teachers Association: Dexter, MI, USA, 2021.
20. Jamali, M.V.; Mirani, A.; Parsay, A.; Abolhassani, B.; Nabavi, P.; Chizari, A.; Khorramshahi, P.; Abdollahramezani, S.; Salehi, J.A. Statistical studies of fading in underwater wireless optical channels in the presence of air bubble, temperature, and salinity random variations. *IEEE Trans. Commun.* **2018**, *66*, 4706–4723. [\[CrossRef\]](#)
21. Jin, Y.; Hu, M.J.; Luo, M.; Luo, Y.; Mi, X.W.; Zou, C.; Zhou, L.W.; Shu, C.F.; Zhu, X.X.; He, J.X.; et al. Beam wander of a partially coherent Airy beam in oceanic turbulence. *J. Opt. Soc. Am. A* **2018**, *35*, 1457–1464. [\[CrossRef\]](#)
22. Guo, Y.; Kong, M.; Sait, M.; Marie, S.; Alkhazragi, O.; Ng, T.K.; Ooi, B.S. Compact scintillating-fiber/450-nm-laser transceiver for full-duplex underwater wireless optical communication system under turbulence. *Opt. Express* **2022**, *30*, 53–69. [\[CrossRef\]](#)
23. Oubei, H.M.; El Afandy, R.T.; Park, K.H.; Ng, T.K.; Alouini, M.S.; Ooi, B.S. Performance evaluation of underwater wireless optical communications links in the presence of different air bubble populations. *IEEE Photon. J.* **2017**, *9*, 7903009. [\[CrossRef\]](#)

**Disclaimer/Publisher's Note:** The statements, opinions and data contained in all publications are solely those of the individual author(s) and contributor(s) and not of MDPI and/or the editor(s). MDPI and/or the editor(s) disclaim responsibility for any injury to people or property resulting from any ideas, methods, instructions or products referred to in the content.